International Journal of Multiphase Flow 34 (2008) 1048–1057

Contents lists available at ScienceDirect

International Journal of Multiphase Flow

journal homepage: www.elsevier.com/locate/ijmulflow

Development of models correlating vibration excitation forces to dynamic characteristics of two-phase flow in a tube bundle

C. Zhang, N.W. Mureithi *, M.J. Pettigrew

BWC/AECL/NSERC Chair of Fluid–Structure Interaction, Department of Mechanical Engineering, École Polytechnique, Montréal, Que., Canada H3T 1J4

ARTICLE INFO

Article history:
Received 29 October 2007
Received in revised form 13 May 2008
Accepted 19 May 2008
Available online 18 July 2008

Keywords:
Two-phase flow
Tube bundle
Quasi-periodic forces
Momentum flux fluctuations
Wake oscillation

ABSTRACT

Recent experiments revealed significant quasi-periodic forces in both the drag and lift directions in a rotated triangular tube bundle subjected to two-phase cross-flow. The quasi-periodic drag forces were found to be related to the momentum flux fluctuations in the main flow path between the cylinders. The quasi-periodic lift forces, on the other hand, are mostly correlated to the oscillation in the wake of the cylinders. In this paper, we develop semi-analytical models for correlating vibration excitation forces to dynamic characteristics of two-phase flow in a rotated triangular tube bundle for a better understanding of the nature of vibration excitation forces. The relationships between the lift or drag forces and the dynamic characteristics of two-phase flow are established through fluid mechanics momentum equations. A model has been developed to correlate the void fraction fluctuation in the main flow path and the dynamic drag forces. A second model has been developed for correlating the oscillation in the wake of the cylinders and the dynamic lift forces. Although still preliminary, each model can predict the corresponding forces relatively well.

1. Introduction

Two-phase cross-flow exists in many shell-and-tube heat exchangers, for instance, in the U-tube region of nuclear steam generators. Flow-induced vibration excitation forces can cause excessive vibration that may result in long-term fretting-wear or fatigue. To prevent such tube failures in heat exchangers, designers and troubleshooters must have guidelines that incorporate flow-induced vibration excitation forces.

In single-phase flow, these forces have been extensively measured and analyzed. They are related to periodic wake shedding and to turbulence generated within the bundle. Experimental data obtained for different kinds of fluids and tube bundles have been satisfactorily compared through the use of adequate data-reduction procedures (Axisa et al., 1990; Blevins, 1991).

In the case of two-phase flows, such extensive studies have not been undertaken, though it is known that there are significant differences between single- and two-phase flows. In particular, the relationship between the two phases must be considered in addition to another parameter which is the void fraction. This results in different flow regimes or patterns of two-phase flow. A few sets of experimental results have been obtained recently, e.g., Axisa et al. (1990), Pettigrew and Taylor (1994), Pettigrew et al. (2005), Nakamura et al. (1995), and Zhang et al. (2006, 2007, 2008). However many questions remain such as the effects of viscosity, surface tension, density ratio and flow regimes. Indeed the main problem is the understanding of the physical mechanism that induces these forces. Detailed flow and vibration excitation force measurements in tube bundles subjected to two-phase cross-flow are required to understand the underlying vibration excitation mechanisms. Some of this work has already been done by Pettigrew et al. (2005) and Zhang et al. (2006, 2007, 2008). The distributions of both void fraction and bubble velocity in rotated triangular tube bundles were obtained (Pettigrew et al., 2005). Significant quasi-periodic forces in both the drag and lift directions were measured (Zhang et al., 2007). The quasi-periodic drag forces appear to be related to the momentum flux fluctuations in the main flow path between the cylinders. The quasi-periodic lift forces, on the other hand, are mostly correlated to the oscillation in the cylinder wakes (Zhang et al., 2008).

The objective of this work is to develop semi-analytical models for correlating these vibration excitation forces to dynamic characteristics of two-phase flow in a rotated triangular tube bundle and understanding the nature of vibration excitation forces. The relationships between the lift or drag forces and the dynamic characteristics of two-phase flow are established through fluid mechanics momentum equations. A model has been developed to correlate the void fraction fluctuation in the main flow path and the dynamic drag forces. A second model has been developed for correlating the oscillation in the wake of the cylinders and the dynamic lift forces.

* Corresponding author. Tel.: +1 514 3404711x4408; fax: +1 514 3404176.
E-mail address: njuki.mureithi@polymtl.ca (N.W. Mureithi).

0301-9322/$ - see front matter © 2008 Elsevier Ltd. All rights reserved.
doi:10.1016/j.ijmultiphaseflow.2008.05.001

2. Experiment

2.1. Experimental set-up

The experiments were done in an air–water loop to simulate two-phase flows. The loop comprised a 25 L/s variable speed pump, a magnetic flow meter, a 2500 L tank, a 250 L/s compressed air supply system and connecting piping as shown in Fig. 1. The water flow was measured via the magnetic flow meter with an overall accuracy of ±0.5% of the reading. The compressed air was injected below a suitably designed mixer to homogenize and distribute the two-phase mixture uniformly below the test-section. The air flow was measured with orifice plates connected to a differential pressure transducer and electronic readout system. The possible measurement error of the orifice plate system is ±1.5% of the nominal value. The loop was operated at room temperature and the pressure in the test-section was slightly above atmospheric.

The test-section, which has essentially a rectangular cross-section (99 × 191 mm), is shown in Fig. 2. It consists of a column of six 38-mm diameter cylinders flanked on either side by half cylinders to simulate essentially the flow path in a large array of cylinders in a rotated triangular configuration. The pitch-to-diameter ratio, P/D, was 1.5 resulting in an inter-cylinder gap of 19 mm which allowed sufficient space for detailed flow measurements. The test-section length-to-gap width ratio is 10, thus, adequate to maintain essentially two-dimensional flow. The measurements were taken at several positions with fiber-optic probes assembled within a traversing mechanism. The tip of the probes could be positioned accurately with a micrometer head.

The probe assemblies were installed at four principal positions in the array as shown in Fig. 2. These positions are henceforth called lower and upper 60° (L60° and U60°) for the narrow gaps between cylinders and lower and upper 90° (L90° and U90°) for the larger flow areas between upstream and downstream cylinders. One cylinder was instrumented with strain gauges to measure the dynamic drag and lift forces due to the two-phase flow.

Each fiber-optic probe has a conical tip and is made of an optical fiber of 170-μm diameter. It acts as a fluid phase sensor based on the different level of light reflection between air and water (Fig. 3). Four probes were used to measure simultaneously the dynamic characteristics of two-phase flow surrounding the instrumented cylinder. Several different probe locations as shown in Fig. 4 were selected for two-phase flow measurements, i.e., LLLL, CCCC, RRRR, etc. Here L, C and R represent the left, center and right positions of probe L60°, L90°, U60° and U90° in the main flow path, respectively. Additionally L_0 is a point on the centerline of the test-section at the U90° probe position. L_1 is about 5 mm from L_0.

Both the dynamic lift and drag forces were measured with a strain gage instrumented cylinder located in the fifth position from the upstream end of the test-section (Fig. 2). The instrumented cyl-

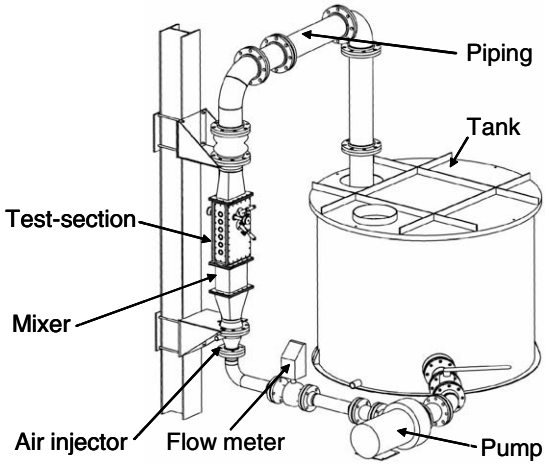

Fig. 1. Test loop.

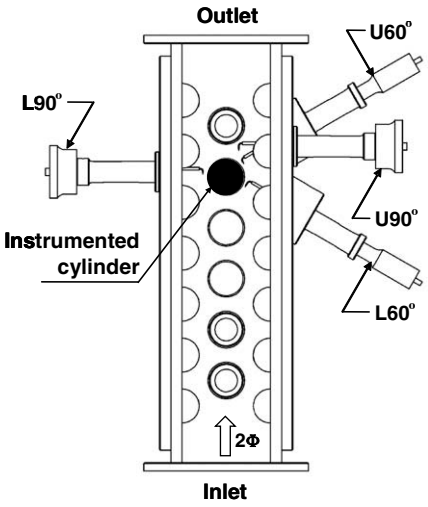

Fig. 2. Test-section.

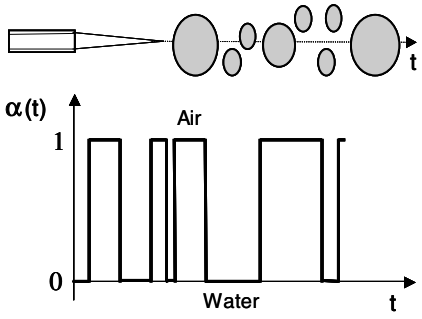

Fig. 3. Ideal two-phase flow signal.

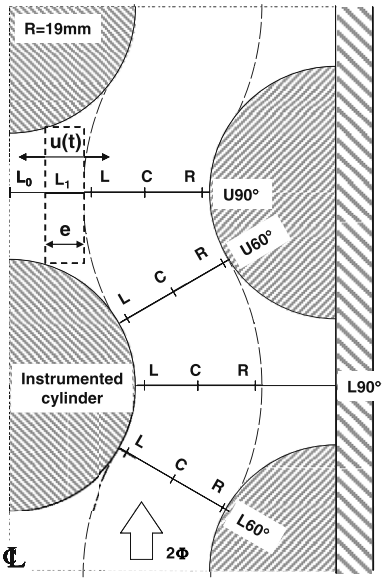

Fig. 4. The main flow path and probe positions for flow measurements.

inder was cantilevered and surrounded by rigid tubes. Two pairs of diametrically opposite strain gages were installed in the cylinder at 90° from each other to measure the forces in the flow direction (drag) and in the direction normal to the flow (lift). The strain gages were connected to strain indicators. The natural frequency of the cantilever cylinders was much higher (i.e., >150 Hz) than the excitation force frequencies such that the cantilever cylinder functioned essentially as a dynamic force transducer. The static strain–force relation was determined via a careful calibration. The estimated accuracy is about ±3% of the reading.

The analysis of two-phase flow-induced vibration requires suitable parameters to express the experimental data. Three flow parameters such as homogeneous void fraction, α, freestream velocity, U_∞, and pitch flow velocity, U_p, are defined as follows:

$$\alpha = \frac{Q_a}{Q_a + Q_w} \tag{1}$$

$$U_\infty = \frac{Q_a + Q_w}{A_\infty} \tag{2}$$

$$U_p = U_\infty \left(\frac{P}{P - D} \right) \tag{3}$$

where Q_a is the volume flow rate of air, Q_w is the volume flow rate of water, P is the pitch or distance between tube centers and D is the tube diameter, respectively.

Two-phase flow, and dynamic lift and drag force measurements were performed simultaneously. Four flow conditions were investigated in detail, i.e., 80% and 90% homogeneous void fractions at a nominal pitch flow velocity, U_p of 5 and 10 m/s. They are located in bubbly flow regime according to Grant's map, which is one of the available flow pattern maps for two-phase cross-flow in cylinder arrays. In Grant's map, bubbly flow and dispersed (spray) flow are probably better described as "continuous flow", while intermittent flow is characterized by periodic flooding (mostly liquid) followed by bursts of mostly gas flow (Taylor et al., 1989). The homogeneous Reynolds numbers corresponding to the four flow condition are presented in Table 1. Both the void probe and the force signals were routinely recorded and analyzed on an OR38 8–32 channel real time multi-analyzer/recorder with NV Gate software coupled to a laptop computer. A sampling rate of 2 kHz was chosen. For each test run, sufficient time (10 min) was allowed for a statistically steady state to be attained. A frequency resolution of 0.125 Hz was used to carry out the spectral analyses of the excitation force and void fraction fluctuation.

Table 1
Homogenous Reynolds numbers for the four flow conditions

Homogenous void fraction α	80%		90%	
Pitch flow velocity U_p (m/s)	5	10	5	10
Homogenous Reynolds number	1.74×10^5	3.48×10^5	1.64×10^5	3.28×10^5

2.2. Experimental results

Experimental results have already been published in Zhang et al. (2008). Typical lift and drag force spectra are shown in Fig. 5. Typical power spectra of the local void fraction fluctuation on the right side, the left side, and along the center line of the main flow path, as well as at positions U90°–L_0 and U90°–L_1 are shown in Figs. 6–9, respectively. Detailed analyses of these results are discussed in Zhang et al. (2008). They are only briefly reviewed here. These results show that

(1) Both the dynamic drag and lift forces and the local void fraction fluctuation spectra show non-random narrow band characteristics.
(2) For the case of 80% void fraction, at 5 m/s pitch flow velocity, the spectra of the local void fraction fluctuation on the right side of the main flow path have a dominant frequency of about 4 Hz (Fig. 6). This dominant frequency is consistent with that of the dynamic drag force (Fig. 5(a)). This clearly indicates a possible dynamic link between the void fraction fluctuation on the right side of the main flow path and the dynamic drag forces.
(3) For the same flow conditions, the spectra of the local void fraction fluctuation on the left side of the main flow path have a dominant frequency of about 11 Hz (Fig. 7). This dominant frequency is consistent with that of the dynamic lift force (Fig. 5(b)). This suggests a possible dynamic relation between the void fraction fluctuation on the left side of the main flow path and the dynamic lift forces.
(4) The spectra of the local void fraction fluctuation along the center line of the main flow path as shown in Fig. 8, appear to be a combination of those on the right and left sides of the main flow path (Figs. 6 and 7).
(5) The spectrum at position U90°–L_0 is very similar to that of the center line of the main flow path (Figs. 9(a) and 8(d)), except that the magnitudes of the power spectral density are higher at L_0. The spectrum at position U90°–L_1 is very similar to that of the left side of the main flow path (Figs. 9(b) and 7(d)) in both magnitude and frequency. This may be explained by the flow observation described below.

Fig. 10(a) is a simplified schematic representation of the flow structure inside a rotated triangular tube bundle. The flow is mostly along the flow path (FP). In between adjacent tubes in the

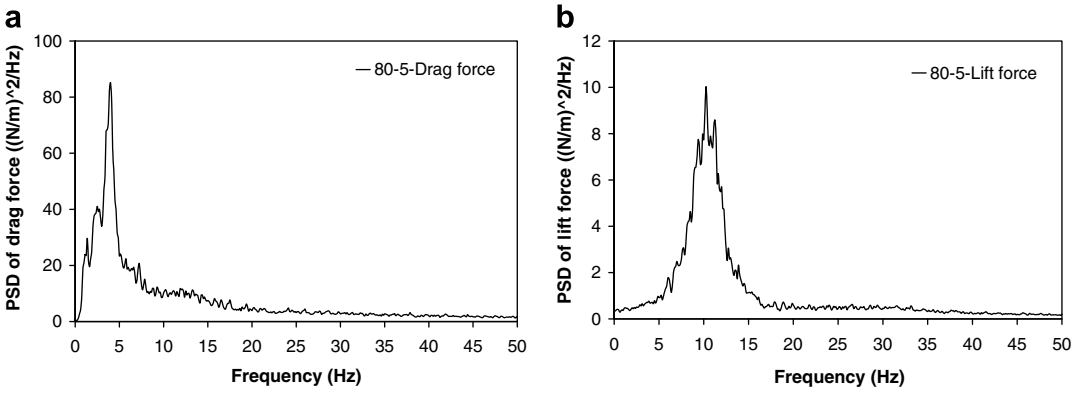

Fig. 5. Typical dynamic force spectra for 80% void fraction at 5 m/s pitch flow velocity: (a) drag force spectra and (b) lift force spectra.

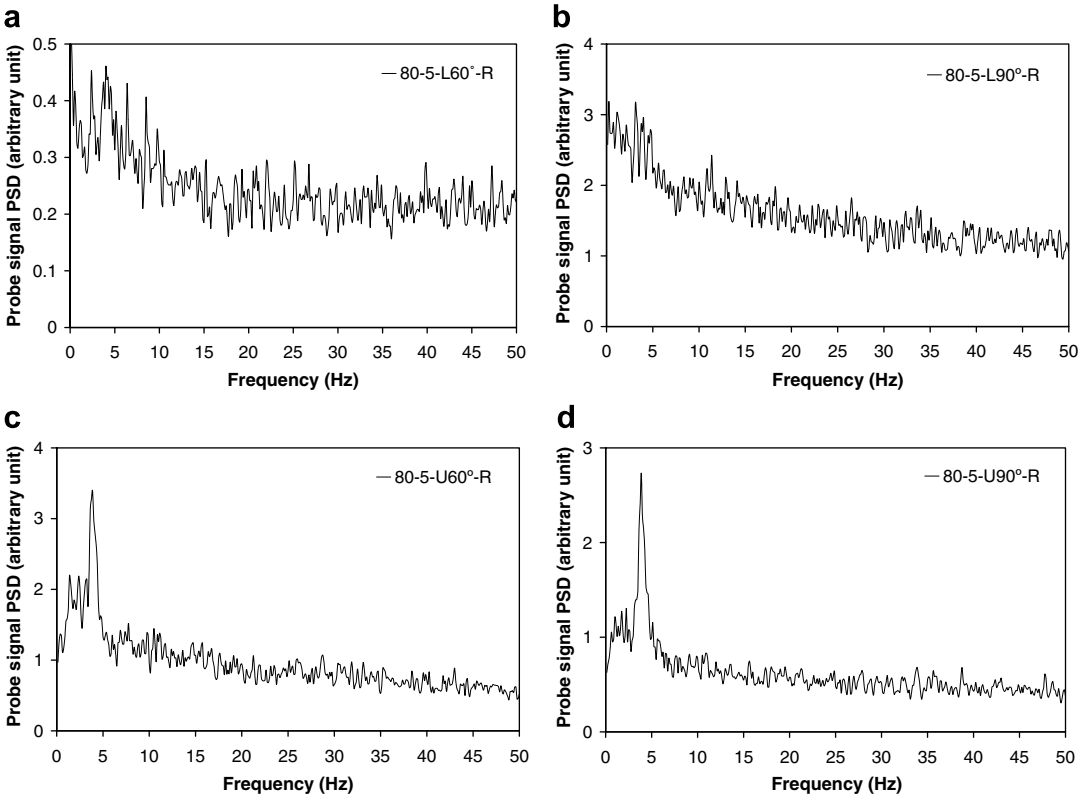

Fig. 6. Power spectra of the local void fraction fluctuation at four different positions on the right side of the main flow path for 80% void fraction at 5 m/s pitch flow velocity: (a) L60° position; (b) L90° position; (c) U60° position; and (d) U90° position.

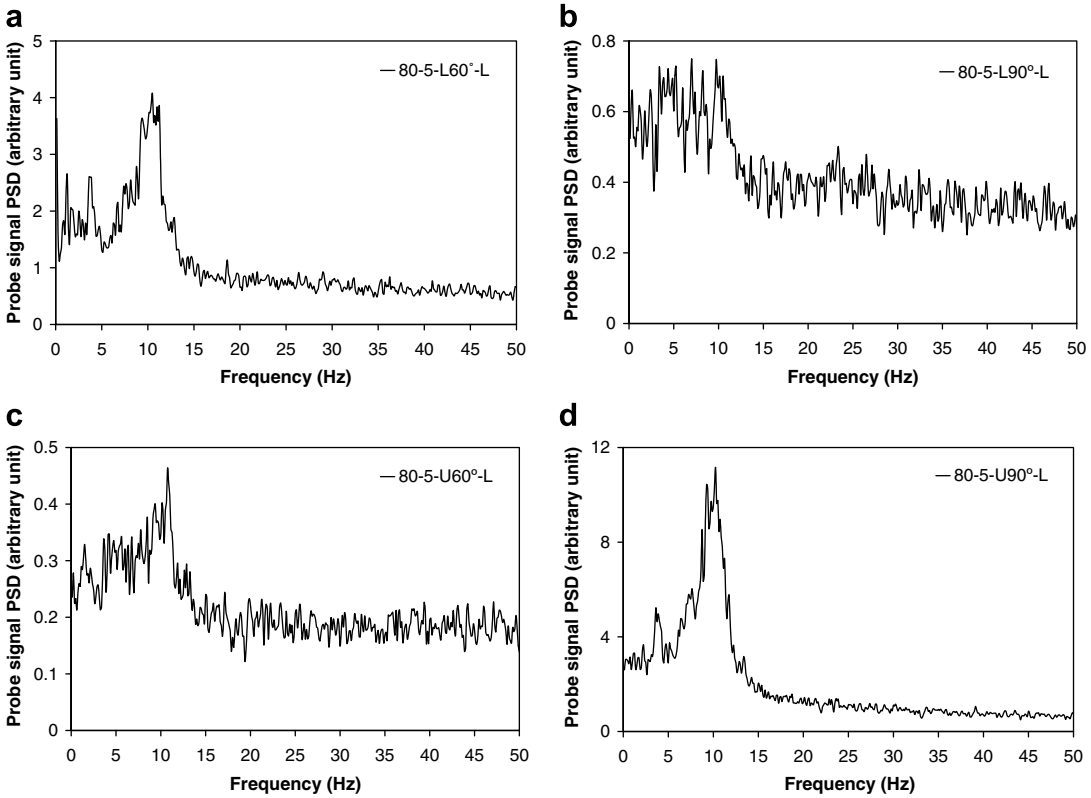

Fig. 7. Power spectra of the local void fraction fluctuation at four different positions on the left side of the main flow path for 80% void fraction at 5 m/s pitch flow velocity: (a) L60° position; (b) L90° position; (c) U60° position; and (d) U90° position.

same column (e.g., Tubes 1 and 2), the flow velocity is much lower than in the flow paths and is taken to be near zero. This zone is called the stagnation zone or recirculation zone (SZ). In two-phase continuous flow, the mixture inside the flow paths appears to be

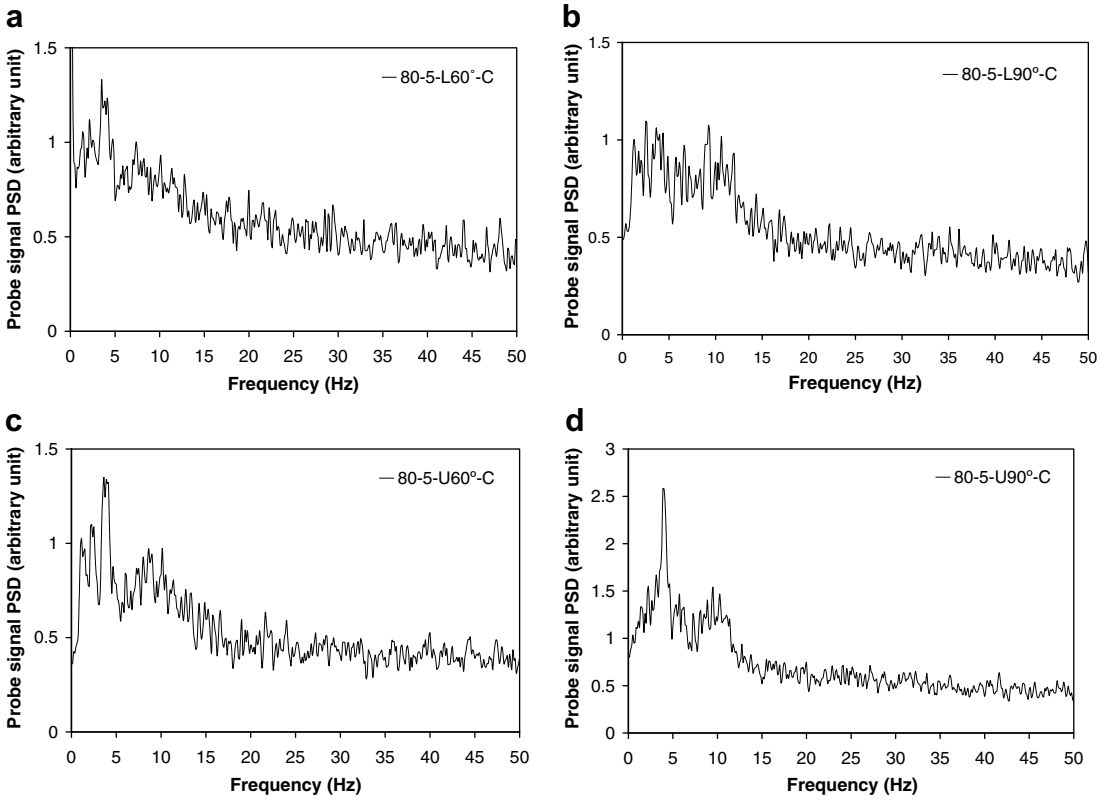

Fig. 8. Power spectra of the local void fraction fluctuation at four different positions along the center line of the main flow path for 80% void fraction at 5 m/s pitch flow velocity: (a) L60° position; (b) L90° position; (c) U60° position; and (d) U90° position.

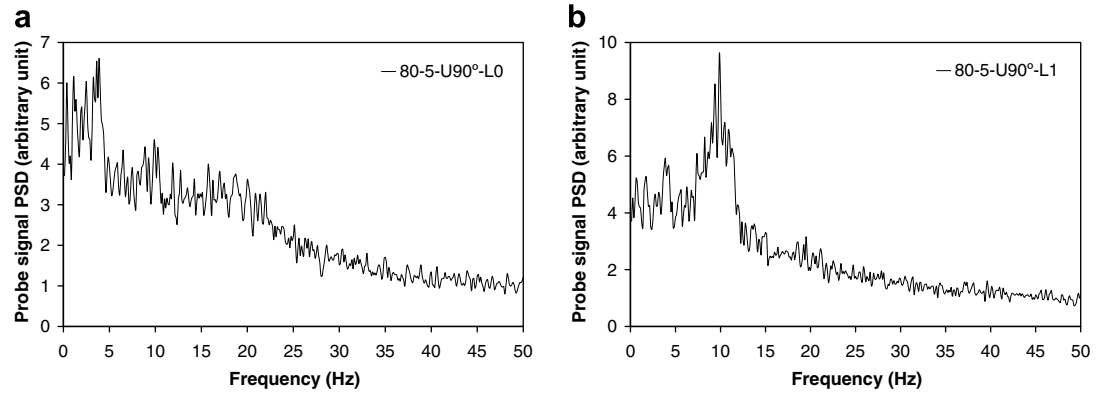

Fig. 9. Power spectra of the local void fraction fluctuation at points L_0 and L_1 of U90° position for 80% void fraction at 5 m/s pitch flow velocity: (a) at point L_0 and (b) at point L_1.

very fine and homogenous. On the other hand, in the stagnation zone (SZ), the two-phase mixture is coarse and non-homogeneous, and transverse oscillations in the wake of the cylinders exist. It is these oscillations that will lead to an oscillatory lift force on the tube. Fig. 10(b) shows a black and white picture of the structure of the two-phase flow inside a rotated triangular array for a high void fraction (95%) and flow velocity of 12 m/s. Except for the tubes themselves, light tones indicate high void fraction mixtures and dark tones indicate very low void fraction two-phase mixtures. From Fig. 10(b), it can be seen that there is a large volume of very low void fraction mixture inside the stagnation zone and that a small portion of the space is occupied by a high void fraction mixtures. Fig. 9(b) therefore shows an instantaneous configuration of the non-homogenous wake during periodic oscillations. A similar phenomenon was observed visually for 80% void fraction at 5 and 10 m/s pitch flow velocities.

The above investigation showed that the quasi-periodic drag and lift forces are generated by different mechanisms. The quasi-periodic drag forces appear related to the momentum flux fluctuations in the main flow path between the cylinder columns. The quasi-periodic lift forces, on the other hand, are mostly correlated to the oscillation in the wake of the cylinders.

Uncertainty analysis on the measured excitation force is briefly given here. One type of uncertainty is caused by the cylinder instrumentation itself. As mentioned in Section 2, the estimated accuracy for the instrumented cylinder is about ±3% of the reading.

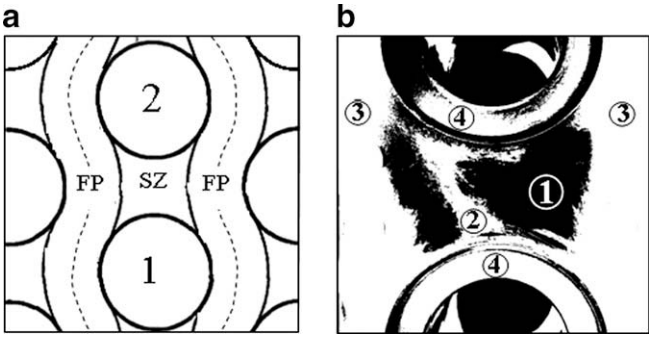

Fig. 10. Two-phase flow structure in a rotated triangular tube bundle: (a) simplified figure (FP, flow path; SZ, stagnation zone) and (b) flow picture (1: low void fraction mixture belonging to the stagnation zone, 2: oscillating high void fraction mixture in stagnation zone, 3: flow path, 4: rigid tubes).

The other uncertainty is due to the method used for power spectral density estimation. In order to reduce the spectral leakage, a sampling rate of 2 kHz was chosen and sufficient time (10 min) was taken for each test run. This allowed us to carry out the spectral analysis of the excitation force with a frequency resolution of 0.125 Hz and 75 segments (40 s for each segment). A Hanning weighting window was also applied to each data segment. Therefore a statistically steady state was attained. The relation between the relative deviation from the mean of the measured drag force and test time for 80% void fraction at 5 m/s pitch flow velocity is shown in Fig. 11. It shows that the relative deviation from the mean of the measured drag force is within the range of ±1% when the test time is longer than 320 s. This implies that 600 s test time (or averaging time) achieves sufficient accuracy. It may be concluded that the uncertainty is mainly caused by the instrumented cylinder and the uncertainty is ±3% in the 95% confidence interval.

After understanding the nature of the observed drag and lift quasi-periodic forces, the logical next step is to develop models to predict these forces starting from the observed dynamic characteristics of two-phase flow.

3. Development of models correlating vibration excitation forces to the dynamic characteristics of two-phase flow

3.1. Model correlating void fraction fluctuations in the main flow path and the dynamic drag forces

The results of the detailed flow measurements indicate that the flow tends to stream between the cylinders and that within that stream the flow velocity is fairly uniform (Pettigrew et al., 2005). Two figures showing, respectively, the distributions of void fraction and bubble velocity in a rotated triangular tube bundle (Pettigrew et al., 2005) are presented in Fig. 12. In fact, the flow path resembles a series of two-dimensional 60° elbows as shown in Fig. 4. This observation serves as the starting point for the development of a model correlating the void fraction fluctuation in the main flow path and the dynamic drag forces.

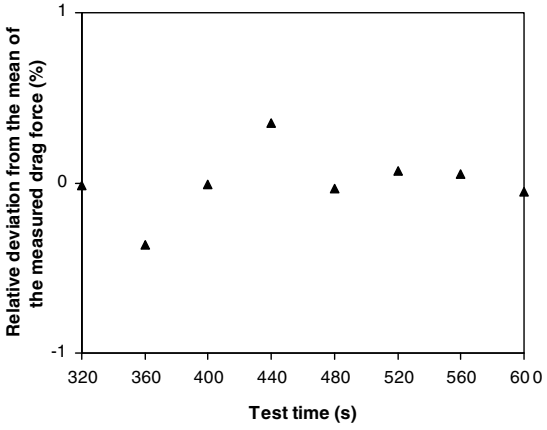

Fig. 11. The relation between the relative deviation from mean of the measured drag force and test time for 80% void fraction at 5 m/s pitch flow velocity.

The vertical forces exerted on the elbows due to two-phase flow may be assumed to be equal to the excitation drag forces on the tubes. There are two 60° elbows surrounding a given tube. The resultant vertical drag force on the tube can be expressed as

$$F_Y(t) = F_{\mathrm{Elbow1},Y}(t) + F_{\mathrm{Elbow2},Y}(t) \tag{4}$$

where $F_Y(t)$, $F_{\mathrm{Elbow},Y}(t)$ are the excitation drag force along the cylinder length (N/m) and the vertical force exerted on the elbow (N/m), respectively, and the subscripts 1, 2 refer to each elbow. The power spectral density, $S_Y(f)$ and the rms value of the measured force are related to the elbow forces. If it is assumed that the elbow forces F Elbow1,$Y(t)$ and $F_{\mathrm{Elbow2},Y}(t)$ are of equal magnitude and fully correlated, then the power spectral density (PSD) and the rms force become

$$S_Y(f) = 4S_{\mathrm{Elbow},Y}(f); \quad F_Y^{\mathrm{rms}}(t) = 2F_{\mathrm{Elbow},Y}^{\mathrm{rms}}(t) \tag{5}$$

The forces exerted on a 60° elbow are determined by considering the control volume shown in Fig. 13. The total force on the control volume is the sum of surface and body forces

$$\vec{F}_{\mathrm{Surface}} + \vec{F}_{\mathrm{Body}} = \int_{\mathrm{CS}} \vec{U} \cdot \rho \vec{U}\, \mathrm{d}\vec{A} + \frac{\partial}{\partial t}\left(\int_{\mathrm{CV}} \rho \vec{U}\, \mathrm{d}V\right) \tag{6}$$

where $\vec{U}$, ρ and V are the gap flow velocity (m/s), two-phase flow mixture density (kg/m^3) and control volume of a 60° elbow (m^3). Following Yih and Griffith (1970) the fluctuating force may be related to the variation with time of the fluid momentum. The elbow force in the Y direction $F_{\mathrm{Elbow},Y}(t)$ is given by Eq. (6) projected in the $\vec{e}_y$ (the vertical unit vector) direction:

$$F_{\mathrm{Elbow},Y}(t) = -\frac{\sqrt{3}}{2}\int_{\mathrm{inlet}} \rho U^2\, \mathrm{d}A + \frac{\sqrt{3}}{2}\int_{\mathrm{outlet}} \rho U^2\, \mathrm{d}A + \frac{\partial}{\partial t}\left(\int_{\mathrm{Elbow}-V} \rho \vec{U}\vec{e}_y\, \mathrm{d}V\right) \tag{7}$$

where the first two surface integrals relate to the flow characteristics at the entrance and exit of the elbow. The third one is a volume integral over the whole fluid domain in the elbow. This is identical to the formulation used by Yih and Griffith (1970) to relate the force exerted by the flow on a tee to variation in void fraction, except that gravity effects are neglected here. It is also equivalent to the formulation developed by Tay and Thorpe (2002, 2004), named Piston Flow Model, except that the pressure gradients due to friction are neglected here. For simplicity, the two-phase flow mixture density is assumed to be homogenous across a section of the elbow and is equal to

$$\rho(t) = \rho_L[1 - \alpha(t)] \tag{8}$$

where ρ_L, $\alpha(t)$ are the liquid density and the instantaneous local void fraction, respectively, and the gas density is neglected. Let us develop term 3 in Eq. (7). In Fig. 10, the angular position $\theta = \frac{\pi/3}{\pi R/3U}\tau$, so, $\mathrm{d}\theta = \frac{U}{R}\,\mathrm{d}\tau$

$$\mathrm{d}V = AR\,\mathrm{d}\theta = AR\frac{U}{R}\,\mathrm{d}\tau = AU\,\mathrm{d}\tau \tag{9}$$

$$\vec{U}\cdot\vec{e}_y = U\sin\left(\frac{\pi}{3} + \theta\right) \tag{10}$$

where R, A, and τ are the radius of the center line of the main flow path (m), gap area (m^2), and the time lag between the inlet and the position (θ) along the elbow (s), respectively.

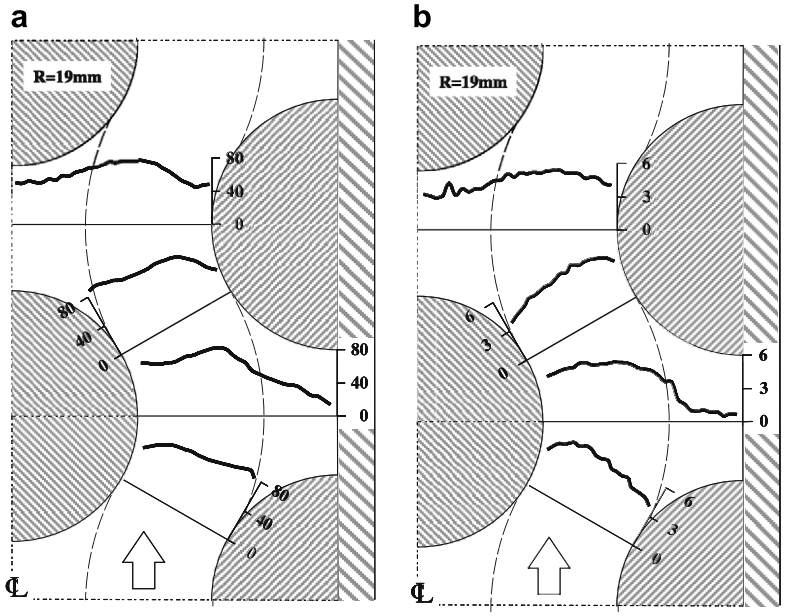

Fig. 12. The distributions of void fraction and bubble velocity in a rotated triangular tube bundle for 80% void fraction at 5 m/s pitch flow velocity: (a) void fraction (%); (b) bubble velocity (m/s) [Pettigrew et al., 2005].

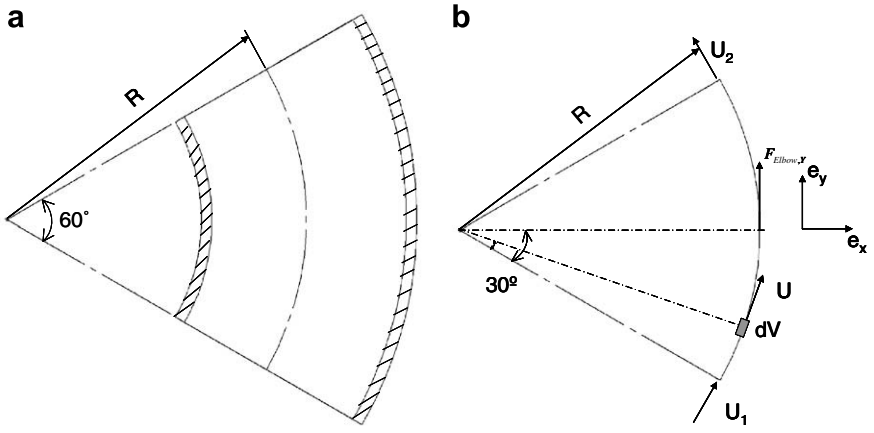

Fig. 13. Sketch of 60° elbow for modeling drag forces.

Introducing Eqs. (9) and (10) into term 3 of Eq. (7), we have

$$\begin{aligned}\frac{\partial}{\partial t}\left(\int_{\text{Elbow}-V}\rho\vec{U}\cdot\vec{e}_y\,\mathrm{d}V\right) &= \frac{\partial}{\partial t}\left\{\int_0^{\delta}\rho_L[1-\alpha(t)]U\sin\left(\frac{\pi}{3}+\theta\right)AU\,\mathrm{d}\tau\right\}\\ &= \rho_L U^2 A\frac{\partial}{\partial t}\left\{\int_0^{\delta}[1-\alpha(t)]\sin\left(\frac{\pi}{3}+\theta\right)\mathrm{d}\tau\right\}\\ &= -\rho_L U^2 A\frac{\partial}{\partial t}\left[\int_0^{\delta}\alpha(t)\sin\left(\frac{\pi}{3}+\theta\right)\mathrm{d}\tau\right]\\ &= -\rho_L U^2 A\left[\int_0^{\delta}\left(\frac{\partial\alpha}{\partial t}\right)_{t-\tau}\sin\left(\frac{\pi}{3}+\theta\right)\mathrm{d}\tau\right]\\ &= -\rho_L U^2 A\left[\int_0^{\delta}\left(\frac{\partial\alpha}{\partial t}\right)_{t-\tau}\sin\left(\frac{\pi}{3}+\frac{U}{R}\tau\right)\mathrm{d}\tau\right]\end{aligned}\tag{11}$$

In the above derivation, it is assumed that the void fraction pattern across the channel is convected by the gap flow velocity U ($U=\frac{\sqrt{3}}{2}U_p$, for rotated triangular tube bundles), thus the density at the inlet, outlet and inside of the elbow are related by time lags only. This means that we could estimate parameters such as $\rho(t)$ and $\alpha(t)$ at any position within the elbow according to the inlet value of $\alpha(t)$. In other words, at any moment t, the void fraction at the inlet is $\alpha(t)$, while at the position (θ) within the elbow it will be $\alpha(t-\tau)$, where τ is the time lag between the inlet and the position (θ) along the elbow. The time lag between the inlet and outlet is $\delta=\pi R/(3U)$. So the void fraction at the outlet will be $\alpha(t-\delta)$. Finally Eq. (7) becomes

$$\begin{aligned}F_{\text{Elbow},y}(t) &= \frac{\sqrt{3}}{2}\rho_L U^2 A[\alpha(t)-\alpha(t-\delta)]\\ &\quad -\rho_L U^2 A\left[\int_0^{\delta}\left(\frac{\partial\alpha}{\partial t}\right)_{t-\tau}\sin\left(\frac{\pi}{3}+\frac{U}{R}\tau\right)\mathrm{d}\tau\right]\end{aligned}\tag{12}$$

Similar equations were also developed by Riverin et al. (2006). Note that the derivative of the instantaneous void fraction $\alpha(t)$ at L60°–C appears in Eq. (12).

The rms value of the elbow force $F^{\mathrm{rms}}_{\mathrm{Elbow},Y}$ could be easily deduced by doing a Fourier Transform of Eq. (12). Let us separate the right side of Eq. (12) into two equations. The first one, $F_{\mathrm{Elbow},YS}(t)$ is due to momentum change at the surface (inlet and outlet), and the second one, $F_{\mathrm{Elbow},YV}(t)$ is due to momentum change within the volume of the elbow.

$$F_{\mathrm{Elbow},YS}(t) = \frac{\sqrt{3}}{2}\rho_L U^2 A[\alpha(t) - \alpha(t-\delta)] \tag{13}$$

$$F_{\mathrm{Elbow},YV}(t) = -\rho_L U^2 A\left[\int_0^{\delta}\left(\frac{\partial\alpha}{\partial t}\right)_{t-\tau}\sin\left(\frac{\pi}{3}+\frac{U}{R}\tau\right)\mathrm{d}\tau\right] \tag{14}$$

We now define the Fourier Transform of $F_{\mathrm{Elbow},YS}(t)$ as $F_{\mathrm{Elbow},YS}(\omega)$, where

$$F_{\mathrm{Elbow},YS}(\omega) = \int_{-\infty}^{+\infty} F_{\mathrm{Elbow},Y1}(t)e^{-j\omega t}\,\mathrm{d}t = \frac{\sqrt{3}}{2}\rho_L U^2 A\alpha(\omega)\left(1-e^{-j\omega\delta}\right) \tag{15}$$

and $F^{*}_{\mathrm{Elbow},YS}(\omega)$ is the complex conjugate of $F_{\mathrm{Elbow},YS}(\omega)$, thus

$$F^{*}_{\mathrm{Elbow},YS}(\omega) = \frac{\sqrt{3}}{2}\rho_L U^2 A\alpha^{*}(\omega)\left(1-e^{j\omega\delta}\right) \tag{16}$$

The PSD of $F_{\mathrm{Elbow},YS}(t)$, $S_{F_{\mathrm{Elbow},YS}}(f_{\pm})$ can be expressed as

$$\begin{aligned} S_{F_{\mathrm{Elbow},YS}}(f_{\pm}) &= \lim_{T\to\infty}\left[\frac{1}{T}F_{\mathrm{Elbow},YS}(f)F^{*}_{\mathrm{Elbow},YS}(f)\right] \\ &= \frac{3}{4}\rho_L^2 U^4 A^2 \lim_{T\to\infty}\left[\frac{1}{T}\alpha(\omega)\alpha^{*}(\omega)\left(1-e^{-j\omega\delta}\right)\left(1-e^{j\omega\delta}\right)\right] \\ &= \frac{3}{2}\rho_L^2 U^4 A^2\left[1-\cos\left(\frac{\pi R}{3U}2\pi f\right)\right]S_{\alpha}(f_{\pm}) \end{aligned} \tag{17}$$

Similarly, the Fourier Transforms of $F_{\mathrm{Elbow},YV}(t)$ is $F_{\mathrm{Elbow},YV}(\omega)$.

$$\begin{aligned} F_{\mathrm{Elbow},YV}(\omega) &= \int_{-\infty}^{+\infty} F_{\mathrm{Elbow},YV}(t)e^{-j\omega t}\,\mathrm{d}t \\ &= -\rho_L U^2 A j\omega\alpha(\omega)\int_0^{\delta}\left[\sin\left(\frac{\pi}{3}+\frac{U}{R}\tau\right)e^{-j\omega\tau}\right]\mathrm{d}\tau \end{aligned} \tag{18}$$

$F^{*}_{\mathrm{Elbow},YV}(\omega)$ is the conjugate of $F_{\mathrm{Elbow},YV}(\omega)$.

$$F^{*}_{\mathrm{Elbow},YV}(\omega) = \rho_L U^2 A j\omega\alpha^{*}(\omega)\int_0^{\delta}\left[\sin\left(\frac{\pi}{3}+\frac{U}{R}\tau\right)e^{j\omega\tau}\right]\mathrm{d}\tau \tag{19}$$

The PSD of $F_{\mathrm{Elbow},YV}(t)$, $S_{F_{\mathrm{Elbow},YV}}(f_{\pm})$ can be expressed as

$$\begin{aligned} S_{F_{\mathrm{Elbow},YV}}(f_{\pm}) &= \lim_{T\to\infty}\frac{1}{T}F_{\mathrm{Elbow},YV}(f)F^{*}_{\mathrm{Elbow},YV}(f) \\ &= \frac{1}{2}\rho_L^2 U^4 A^2(2\pi f)^2 S_{\alpha}(f_{\pm})\left[\frac{1-\cos\left(\frac{\pi}{3}+\frac{\pi R}{3U}2\pi f\right)}{\left(\frac{U}{R}+2\pi f\right)^2}\right. \\ &\quad \left.+\frac{1-\cos\left(\frac{\pi}{3}-\frac{\pi R}{3U}2\pi f\right)}{\left(\frac{U}{R}-2\pi f\right)^2}+2\frac{\cos\left(\frac{\pi R}{3U}2\pi f\right)+\cos\frac{2\pi}{3}}{\left(\frac{U}{R}\right)^2-(2\pi f)^2}\right] \end{aligned} \tag{20}$$

Recalling Eqs. (12)–(14), we have

$$F_{\mathrm{Elbow},Y}(t) = F_{\mathrm{Elbow},YS}(t) + F_{\mathrm{Elbow},YV}(t) \tag{21}$$

The power spectral density of $F_{\mathrm{Elbow},Y}(t)$, $S_{F_{\mathrm{Elbow},Y}}(f_{\pm})$ can be expressed as follows:

$$S_{F_{\mathrm{Elbow},Y}}(f_{\pm}) = S_{F_{\mathrm{Elbow},YS}}(f_{\pm}) + S_{F_{\mathrm{Elbow},YV}}(f_{\pm}) + S_{F_{\mathrm{Elbow},YSV}}(f_{\pm}) + S_{F_{\mathrm{Elbow},YVS}}(f_{\pm}) \tag{22}$$

The last two terms of Eq. (22) are cross-power spectral densities between the volume force $F_{\mathrm{Elbow},YS}(t)$ and the surface force $F_{\mathrm{Elbow},YV}(t)$. They are neglected being secondary terms.

$$S_{F_{\mathrm{Elbow},Y}}(f_{\pm}) = S_{F_{\mathrm{Elbow},YS}}(f_{\pm}) + S_{F_{\mathrm{Elbow},YV}}(f_{\pm}) \tag{23}$$

The mean square (MS) value of $F_{\mathrm{Elbow},Y}(t)$, $\overline{F}^2_{\mathrm{Elbow},Y}(t)$ will be

$$\begin{aligned} \overline{F}^2_{\mathrm{Elbow},Y}(t) &= \int_0^{\infty} S_{F_{\mathrm{Elbow},Y}}(f)\,\mathrm{d}f \\ &= \frac{1}{2}\rho_L^2 U^4 A^2\int_0^{\infty} S_{\alpha}(f)\left[3\left(1-\cos\frac{\pi R}{3U}2\pi f\right)\right]\mathrm{d}f \\ &\quad +\frac{1}{2}\rho_L^2 U^4 A^2\int_0^{\infty} S_{\alpha}(f) \\ &\quad \times(2\pi f)^2\left[\frac{1-\cos\left(\frac{\pi}{3}+\frac{\pi R}{3U}2\pi f\right)}{\left(\frac{U}{R}+2\pi f\right)^2}\right]\mathrm{d}f+\frac{1}{2}\rho_L^2 U^4 A^2 \\ &\quad \times\int_0^{\infty} S_{\alpha}(f)(2\pi f)^2\left[\frac{1-\cos\left(\frac{\pi}{3}-\frac{\pi R}{3U}2\pi f\right)}{\left(\frac{U}{R}-2\pi f\right)^2}\right]\mathrm{d}f \\ &\quad +\frac{1}{2}\rho_L^2 U^4 A^2\int_0^{\infty} S_{\alpha}(f) \\ &\quad \times(2\pi f)^2\left[2\frac{\cos\left(\frac{\pi R}{3U}2\pi f\right)+\cos\frac{2\pi}{3}}{\left(\frac{U}{R}\right)^2-(2\pi f)^2}\right]\mathrm{d}f \end{aligned} \tag{24}$$

$S_{\alpha}(f)$ in Eq. (24) could be obtained directly from probe signal at L60° (position C).

Introducing Eq. (24) into Eq. (5), the rms value of the resultant vertical drag force on the tube will be

$$F^{\mathrm{rms}}_{Y}(t) = 2\sqrt{\overline{F}^2_{\mathrm{Elbow},Y}(t)} \tag{25}$$

A computer code was programmed using Eqs. (24) and (25) for estimating the drag force according to the void signal (probe signal of L60°–C).

The resulting rms values are presented in Table 2, where comparison with the direct measurements of the forces is made. Although the measured values are lower than the calculations, they are both within the same order of magnitude. An important reason for the difference is that the coherence between void fraction fluctuation at L60°–C and drag forces is relatively high only in the range 0–10 Hz (Zhang et al., 2008). One of the figures showing that coherence (Zhang et al., 2008) is presented in Fig. 14. Beyond 10 Hz, the coherence is extremely low. If only the frequency range 0–10 Hz is considered for the measured and estimated forces, much better agreement is found as shown in Table 3. This

Table 2
Comparison between measured and estimated rms drag forces (N/m) within 0–20 Hz

Pitch flow velocity U_p (m/s)	α = 80%		α = 90%	
	Measured	Estimated	Measured	Estimated
5	18.1	51.5	13.7	54.7
10	31.9	49	20.3	50.9

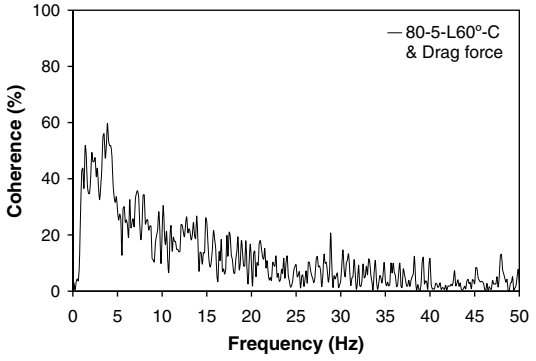

Fig. 14. Coherences between the local void fraction fluctuation at L60°–C and the dynamic drag force for 80% void fraction at 5 m/s pitch flow velocity.

Table 3
Comparison between measured and estimated rms drag forces (N/m) within 0–10 Hz

Pitch flow velocity U_p (m/s)	α = 80%		α = 90%	
	Measured	Estimated	Measured	Estimated
5	15.9	21.1	12.4	23.9
10	28.8	20.7	18.5	20.3

and other possible explanations are currently being considered which should lead to a more refined model.

3.2. Model correlating oscillations in the wake of the cylinders and the dynamic lift forces

A model for correlating oscillations in the wake of the cylinders and the dynamic lift forces is also developed. Although the mechanism for the oscillation in the wake of the cylinders is not as yet completely understood, it may be similar to oscillations associated with low frequency mechanisms for some structures in single-phase flow. It has been hypothesized to be due to an imbalance between flow entrained by the separated shear layer and that returned to the separation zone at reattachment (Rockwell, 1983). For the purpose of model development, based on our visualizations, video-photography and fiber-optic probe measurements, this wake oscillation could be thought as two low void shear layers self-excited transversely between the upstream and downstream cylinders. This characteristic of wake oscillation is assumed to be sustained when this wake flow passes through the main flow path.

Only the oscillation at the dominant frequency is taken into account on here, so the motion and velocity equations of the oscillating wake will be

$$x(t) = \frac{1}{2} e \sin(2\pi f t); \quad u(t) = \pi e f \cos(2\pi f t) \tag{26}$$

where e, f are the width of the wake (Fig. 4) and dominant frequency, the oscillating amplitude of the wake was assumed to be half of e as deduced from the experiments.

The horizontal forces exerted on the elbows due to the wake oscillation may be assumed to be equal to the excitation lift forces on the tubes. There are two 60° elbows surrounding the tube. The resultant horizontal lift force on the tube can be expressed as

$$F_X(t) = F_{\text{Elbow1},X}(t) + F_{\text{Elbow2},X}(t) \tag{27}$$

where $F_X(t)$, $F_{\text{Elbow},X}(t)$ are the excitation lift force along the cylinder length (N/m) and the horizontal force exerted on the elbow (N/m), respectively, and the subscripts 1, 2 refer to each elbow. The rms value of the measured force is related to that of the elbow forces. If it is assumed that the elbow forces $F_{\text{Elbow1},X}(t)$ and $F_{\text{Elbow2},X}(t)$ are of equal magnitude and not correlated, then the rms force becomes

$$F_X^{\text{rms}}(t) = \sqrt{2} F_{\text{Elbow},X}^{\text{rms}}(t) \tag{28}$$

The control volume for the evaluation of the forces exerted on a 60° elbow is considered as shown in Fig. 15. The fluctuating lift force may be related to the variation with time of the wake momentum in a 60° elbow. The elbow force in the X direction $F_{\text{Elbow},X}(t)$ is given by Eq. (6) projected in the $\vec{e}_x$ (the horizontal unit vector) direction.

$$F_{\text{Elbow},X}(t) = \frac{\partial}{\partial t}\left[\int_{\text{Elbow}-V} \rho_L \vec{u}(t)\vec{e}_x \, \mathrm{d}V\right] \tag{29}$$

The term on the right hand is a volume integral over the whole fluid domain in the elbow. Based on experiments, the mean radius of the wake in the main flow path, R_1 was taken as the radius of the tube plus wake width. In the 60° elbow, the wake oscillation velocity $\vec{u}(t)$ is just in the normal or transverse direction and is assumed to keep the same oscillation amplitude as that in between upstream and downstream cylinders. The term related to the surface integral is zero due to $\vec{u}(t)$ being perpendicular to $d\vec{A}$. Further derivation is given as follows:

$$\begin{aligned} F_{\text{Elbow},X}(t) &= \frac{\partial}{\partial t}\left[\int_{\text{Elbow}-V} \rho_L \vec{u}(t)\vec{e}_x \, \mathrm{d}V\right] \\ &= \frac{\partial}{\partial t}\left[\int_0^{\frac{\pi}{3}} \rho_L \pi e f \cos(2\pi f t)\cos(\frac{\pi}{6} - \theta) e R_1 \, \mathrm{d}\theta\right] \\ &= \frac{\partial}{\partial t}\left\{\rho_L \pi e^2 R_1 f \cos(2\pi f t)\left[-\sin\left(\frac{\pi}{6} - \theta\right)\right]_0^{\frac{\pi}{3}}\right\} \\ &= -2\pi^2 \rho_L R_1 e^2 f^2 \sin(2\pi f t) \end{aligned} \tag{30}$$

Introducing final result of Eq. (30) into Eq. (28), the rms value of the resultant horizontal lift force on the tube will be

$$F_X^{\text{rms}}(t) = -2\sqrt{2}\pi^2 \rho_L R_1 e^2 f^2 \sin(2\pi f t) \tag{31}$$

If the periodic frequency is introduced in Eq. (31), the rms value of the resultant horizontal lift force can be estimated.

The corresponding rms values are presented in Table 4, and compared to the direct measurement of the force. Although the measured values are generally lower than the calculations, they are both reasonably close for a first attempt at estimating these forces deriving from a complex two-phase flow phenomenon.

The two models above are applicable to the other rows of tube bundle except the first and last rows. This is because the flow surrounding the first and last row cylinders is different than that surrounding the inner row cylinders.

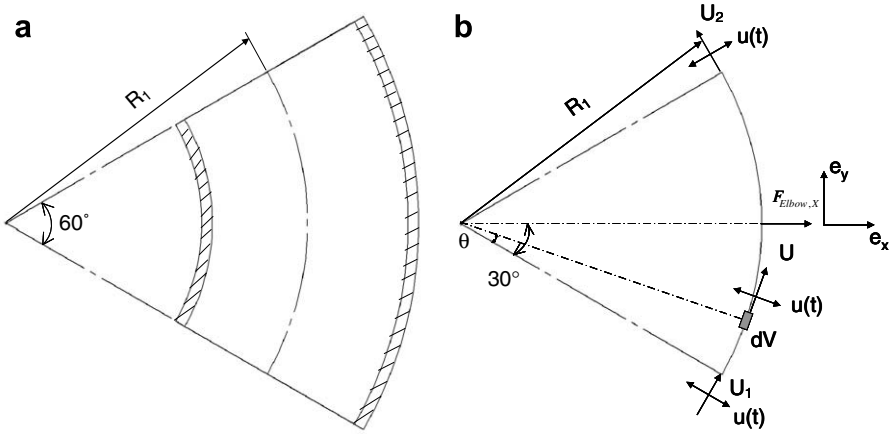

Fig. 15. Sketch of 60° elbow for modeling lift forces.

Table 4
Comparison between measured and estimated rms lift forces (N/m) at the dominant frequency

Pitch flow velocity U_p (m/s)	α = 80%		α = 90%	
	Measured	Estimated	Measured	Estimated
5	1.3	1.65	1.13	1.04
10	2.42	4.34	1.69	2.31

4. Conclusion

Quasi-periodic drag and lift forces were measured on an array of cylinders subjected to two-phase flow. Measurements of the dynamic characteristics of the two-phase flow indicate that quasi-periodic drag and lift forces are generated by different mechanisms that have not been reported previously. The quasi-periodic drag forces were found to be related to the momentum flux fluctuations in the main flow path between the cylinders. These momentum flux fluctuations are caused by the void fraction fluctuations in the main flow path between the cylinders. The quasi-periodic lift forces, on the other hand, are mostly correlated to oscillations in the wake of the cylinders. The relationships between the lift or drag forces and the dynamic characteristics of two-phase flow are established through fluid mechanics momentum equations. A model has been developed to correlate the void fraction fluctuation in the main flow path and the dynamic drag forces. A second model has been developed for correlating the oscillation in the wake of the cylinders and the dynamic lift forces. Although further development is needed, these preliminary models are encouraging since plausible prediction is made.

Acknowledgments

The authors are grateful to Dragos Pamfil for the test-section design and the development of the fiber-optic probes. Thanks are also due to Thierry Lafrance, Bénedict Besner and Nour Aimène for their help throughout the project.

References

Axisa, F., Antunes, J., Villard, B., 1990. Random excitation of heat exchanger tubes by cross-flows. J. Fluids Struct. 4, 321–341.
Blevins, R.D., 1991. Flow-Induced Vibration, second ed. Van Nostrand Reinhold, New York.
Nakamura, T., Fujita, K., Kowanishi, N., Yamaguchi, N., Tsuge, A., 1995. Study on the vibration characteristics of a tube array caused by two-phase flow, part 1: random vibration. J. Fluids Struct. 9, 519–538.
Pettigrew, M.J., Taylor, C.E., 1994. Two-phase flow-induced vibration: an overview. ASME J. Press. Vessel Technol. 116, 233–253.
Pettigrew, M.J., Zhang, C., Mureithi, N.W., Pamfil, D., 2005. Detailed flow and force measurements in a rotated triangular tube bundle subjected to two-phase cross-flow. J. Fluids Struct. 20, 567–575.
Riverin, J.L., de Langre, E., Pettigrew, M.J., 2006. Fluctuating forces caused by internal two-phase flow on bends and tees. J. Sound Vib. 298, 1088–1098.
Rockwell, D., 1983. Oscillation of impinging shear layers. AIAA J. 21, 645–664.
Taylor, C.E., Currie, I.G., Pettigrew, M.J., Kim, B.S., 1989. Vibration of tube bundles in two-phase cross-flow. Part 3: turbulent induced excitation. ASME J. Press. Vessel Technol. 111, 488–500.
Tay, B.L., Thorpe, R.B., 2004. Effect of liquid physical properties on the forces acting on a pipe bend in gas–liquid slug flow. Chem. Eng. Res. Des. 82, 344–356.
Tay, B.L., Thorpe, R.B., 2002. Forces on a pipe bend due to slug flow. In: Proceeding of the 3rd North American Multiphase Technology Conference, Banff, pp. 281–300.
Yih, T.S., Griffith, P., 1970. Unsteady momentum fluxes in two-phase flow and the vibration of nuclear system components. In: Proceeding of the International Conference on Flow-Induced Vibration in Reactor System Components, Argonne Ill., Report ANL-7685, pp. 91–111.
Zhang, C., Pettigrew, M.J., Mureithi, N.W., 2006. Quasi-periodic vibration excitation mechanism due to two-phase cross flow in steam generator tube bundles. In: Proceedings of 5th CNS International Steam Generator Conference, Toronto, Canada, CD-ROM, #26.
Zhang, C., Pettigrew, M.J., Mureithi, N.W., 2007. Vibration excitation force measurements in a rotated triangular tube bundle subjected to two-phase cross flow. ASME J. Press. Vessel Technol. 129, 21–27.
Zhang, C., Pettigrew, M.J., Mureithi, N.W., 2008. Correlation between vibration excitation forces and the dynamic characteristics of two-phase cross flow in a rotated triangular tube bundle. ASME J. Press. Vessel Technol. 130. 011301(1–10).